Force-closure orchard dexterous hand grasping model

Xiulan Bao[1], Mengtao Ren[1], Xiaojie Ma[1], Biyu Chen[1], Yougang Bao[1], Jincheng Mao[2*]

(1. *College of Engineering, Huazhong Agricultural University, Wuhan 430070, China*;
2. *School of Mechanical and Electrical Engineering, Wuhan Institute of Technology, Wuhan 432200, China*)

Abstract: The digital orchard is an important trend for the future development of orchards towards intelligentization. The current wide variety of orchard gripping objects with different sizes and material characteristics brings challenges for gripping operations. In order to improve the versatility and dexterity of the orchard end-effector, a humanoid 14-degree-of-freedom orchard dexterous hand is designed for agronomic operations. An optimal design scheme of the orchard dexterous hand combining orchard gesture analysis and human hand structure is proposed, and the design of the modular fingers, palm, and overall structure of the orchard dexterous hand is completed. The orthogonal and inverse kinematics model of the dexterous hand is established to analyze the motion space of the fingertips, and the dexterity of the orchard dexterous hand is verified by combining with the Kapandji test. The equivalent distribution model of the contact force is solved according to the Hertz theory, and the grasping matrix is established based on the friction surface contact model to realize force-closure, which describes the relationship between the finger and the object being grasped in the configuration. The experimental platform of dexterous hand in the orchard is built, and the experiments of gesture formation, grasping, and contact force testing are carried out. The results show that the dexterous hand can form all kinds of gestures commonly used in the orchard and can grasp spherical fruit with diameters of 26-90 mm, masses of 11-238 g, and all kinds of orchard-specific working tools; for navel oranges with masses of 234 g, the dexterous hand can realize stable grasping under different gestures. This provides a theoretical basis and technical support for the realization of complex agronomy in orchards.

Keywords: digital orchard, dexterous hand, orchard gesture, force-closure
DOI: 10.25165/j.ijabe.20251804.8925

Citation: Bao X L, Ren M T, Ma X J, Chen B Y, Bao Y G, Mao J C. Force-closure orchard dexterous hand grasping model. Int J Agric & Biol Eng, 2025; 18(4): 139–148.

1 Introduction

In order to promote the long-term development of the fruit industry, it is crucial to minimize labor costs, reduce the dependence on manual labor, and realize the mechanization and intelligence of the whole orchard operation[1-3]. Among these, it is essential to study end-effectors suitable for gripping fruits of different sizes and performing various agronomic operations[4].

Different fruits have different shape characteristics and different gripping mechanical properties, and the harvesting methods required in agronomy vary widely[5-8]. At the same time, different crops in the orchard at different stages of agronomic indicators are diverse[9,10]; for example, citrus, lychee, and other evergreen fruit trees need thinning, pruning, and other agronomic operations. In addition, the internal space of these fruit trees is canopy closing, which is not conducive to mechanical orchard operations. Therefore, at present these agronomic operations are still primarily carried out with manually gripped tools[11]. Zhou et al.[12] developed a pneumatic end-effector with three four-chamber fingers, engineered according to the biophysical properties of tomatoes. Lin et al.[13] designed an end-effector for real-time harvesting and grading by collecting spectral signals. Gao et al.[14] designed a pneumatic finger-type end-effector for cherry tomato harvesting to improve operational efficiency. Wei et al.[15] designed a three-finger underdriven end-effector for citrus picking. Zahid et al.[16] developed a three-degree-of-freedom pruning end-effector for cutting apple branches. Jongpyo et al.[17] developed a pneumatic cutter end-effector for cutting the stems of cherry tomatoes. In summary, most of the existing end-effectors are designed for specific fruits and agronomy and suffer from low utilization and high cost. Therefore, adopting a versatile end-effector to complete a variety of precision agronomic operations will significantly improve the utilization rate of end-effectors in orchards and is an effective way to improve the mechanization level of orchard operations[18].

As an end-effector designed to mimic the human hand, the dexterous hand can accomplish a variety of dexterous grasps and perform complex operations[19]. The research on dexterous hands is relatively mature[20-23]. Tao et al.[24] designed a three-finger, nine-degree-of-freedom dexterous hand based on gesture proto-language analysis, simplifying the complex human-like five-finger hand system. Kim et al. developed an integrated link-driven dexterous hand by adopting a variety of drive modes such as direct motor drive, tendon drive, and link drive[25]. Some companies manufacture commercialized multi-fingered dexterous hands, such as the Shadow dexterous hand from Shadow Robot (UK)[26] and the SF5H hand from SCHUNK (Germany)[27]. In addition to industry applications, multi-fingered dexterous hands have begun to be used in rehabilitation training, life socialization, and other fields[28]. However, the existing dexterous hand has a complex structure, a precise mechanism, and poor anti-interference ability, leading to a

Received date: 2024-03-15 **Accepted date:** 2025-04-06
Biographies: **Xiulan Bao**, PhD, Associate Professor, research interest: agricultural robot, Email: orchidbaoxl@mail.hzau.edu.cn; **Mengtao Ren**, MS, research interest: Robot operation grasping and control, Email: 15736896186@163.com; **Xiaojie Ma**, MS, research interest: Robot collaboration and control, Email: mxj3023@163.com; **Biyu Chen**, MS, research interest: agricultural robot, Email: 1669729408@qq.com; **Yougang Bao**, MS, research interest: agricultural robot, Email: 19970039856@163.com.
***Corresponding author: Jincheng Mao**, PhD, Associate Professor, research interest: Robotic Measurement Processing and Applications; Mailing address: Tel: +86-13871229154, Email: 88971437@qq.com.

high failure rate and increased production cost when directly applied to orchards.

In order to improve the versatility and dexterity of the orchard end-effector to realize specific grasping and manipulation tasks in the orchard, we propose a design scheme that combines orchard gesture analysis and human-like hand structure to design the orchard dexterous hand, establish a kinematic model and grasping model, analyze its working performance, and build an experimental platform to carry out the functional verification of the orchard dexterous hand as well as the contact force testing experiments.

2 Orchard dexterous hand gesture analysis and structural design

2.1 Analysis of orchard gestures

First, a detailed record of the operational tasks in the orchard that require human hands and their various gestures summarizes the common gestures used in the orchard. There is a big difference in the way different fruits are harvested. Apples, pears, etc., are mostly lifted upward along the fruit stalk; kiwifruit are broken mainly by gently pressing on the fruit stalk; peaches are mostly twisted by gently grasping the fruit; and citrus are picked mainly by the two-shear method. When thinning flowers, pruning, and performing other agronomic operations, operating tools are usually used to assist in the operation. The tools used for grasping the part are essentially cylindrical, based on a stabilized grip, and operated through the movement of the finger joints. Based on the commonly used gestures in the orchard, combined with the Feix grasping classification table[29-31], they are merged, streamlined, and categorized according to the number of fingers required to form the gesture, as well as the category of the grasping task, to produce a classification table of the orchard grasping gestures, as shown in Figure 1. Table capture objects are common fruits and commonly used tools in the orchard. There are a total of 13 gestures, which cover the basis of the orchard operation gestures. Compared to the Feix capture classification table, the gesture number is significantly reduced, which is conducive to the analysis of the orchard gesture characteristics.

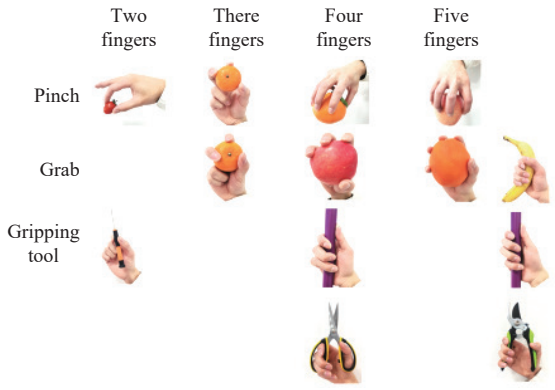

Figure 1 Orchard grasping gesture classification table

As shown in Figure 1, the four-finger and five-finger gestures have similar functionalities, with the little finger in the five-finger gesture serving only an auxiliary role. Therefore, the little finger is omitted, and the design is optimized for a four-finger dexterous hand. When forming gestures, each finger moves flexibly and in coordination with the others. Based on the movement patterns of the joints in human hands and fingers, the degrees of freedom of the joints in dexterous hands and fingers are reproduced and modularized. When the index finger and ring finger are used together to form a pinching or grasping gesture, the lateral swing angles of the two fingers are essentially the same. Coupling the lateral swing of the index finger and ring finger while keeping the middle finger stationary increases the grasping space of the orchard dexterous hand and reduces system complexity. Based on the analysis results, the structural design of the orchard dexterous hand is carried out, with the joint structure layout shown in Figure 2.

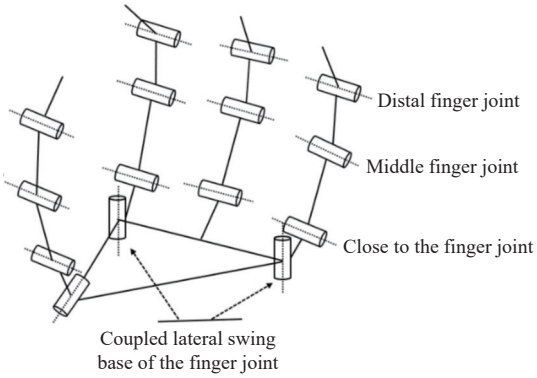

Figure 2 Articular structure layout of orchard dexterous hand

2.2 Overall structural design

The orchard dexterous hand finger is arranged in an imitation human hand style, and the freedom of the human hand is restored as much as possible. The thumb is arranged on the side of the palm, and the remaining three fingers are evenly spaced on the top of the palm and opposite the thumb. The thumb, index finger, and ring finger contain four joints: the base joint, the proximal joint, the middle joint, and the distal joint, of which the base joint is a side-swinging joint, and the base joints of the index and ring fingers are coupled with the side-swinging joints. The middle finger contains three joints with no base joints. The orchard dexterous hand has 14 degrees of freedom overall, with two sets of base joints for side-swing freedom and the remaining 12 joints for bending freedom. The orchard dexterous hand consists of four fingers and palms; the main structure is shown in Figure 3. The orchard dexterous hand is driven by 14 motors, which control the opening and closing of the four fingers and the bending of each joint, respectively, to realize the purpose of operation through gesture formation.

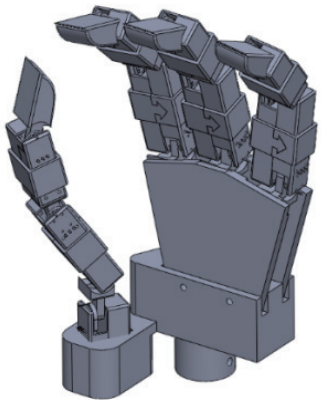

Figure 3 Structure of orchard dexterous hand

2.3 Finger modular design

In order to simplify the overall structural design of the orchard dexterous hand, reduce the design and manufacturing costs, and improve the ease of maintenance of the system, the fingers are modularized, and the mechanical structure of the four fingers is the

same. Take the index finger as an example. As shown in Figure 4, modeled on the tip of a human finger, the lower surface and side of the fingertip are designed with curved surface curvature to increase the mating area so that the tip of the finger and the object fit each other to achieve stable grasping. A DC motor is built into the middle knuckle to drive the bending motion of the distal knuckle. The proximal knuckle has two built-in DC motors, which are placed oppositely close to each other in order to reduce the size of the proximal knuckle and drive the bending motion of the middle and proximal joints, respectively, which restores the bending motion of the human finger and better forms the familiar gestures of the orchard. The fixation of the middle and proximal knuckles is designed as a removable snap fixation, which makes it easy to remove the fingers for maintenance and replacement.

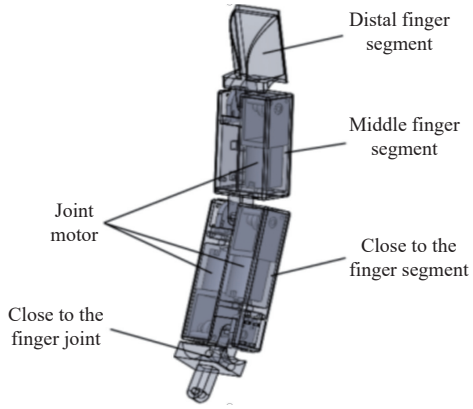

Figure 4 Orchard dexterous hand finger structure

2.4 Side pendulum coupling mechanism design

The drive mechanism of the base joints of the index and ring fingers is coupled in the palm, and the lateral pendulum motion of the two joints is controlled by a motor. The design of the coupling structure is shown in Figure 5. The rotary motion of the motor is converted into linear motion under the limitation of the driving connecting rod and the bar groove. When the connecting rod moves upward along the groove, the index finger and ring finger open sideways at the same time, and vice versa: the index finger and ring finger close at the same time, realizing the lateral pendulum motion of the two fingers at the same time to reduce one degree of freedom. The angle of the lateral pendulum is ±20°.

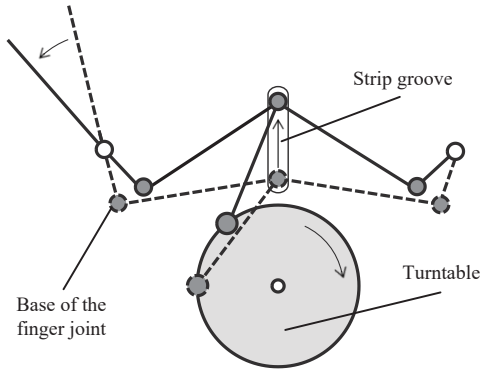

Figure 5 Lateral pendulum coupling motion schematic

3 Kinematics and dexterity analysis of orchard dexterous hands

3.1 Positive kinematics modeling

Figure 6 shows the coordinate system of the orchard dexterous hand. A global coordinate system $\boldsymbol{H}\{x, y, z\}$ is established at the base joint of the middle finger, with the finger direction in the X-direction and the direction from the base joint of the middle finger to the base joint of the ring finger in the Z-direction. The base coordinate system is established at the base joint of each finger, and the thumb, index finger, middle finger, and ring finger base coordinate systems are defined as T, I, M, and R in turn. A fingertip coordinate system was established at the fingertip point in the order of the base coordinate system (#0), the lateral pendulum base joint (#1), the proximal joint (#2), the middle joint (#3), the distal joint (#4), and the fingertip point (#5).

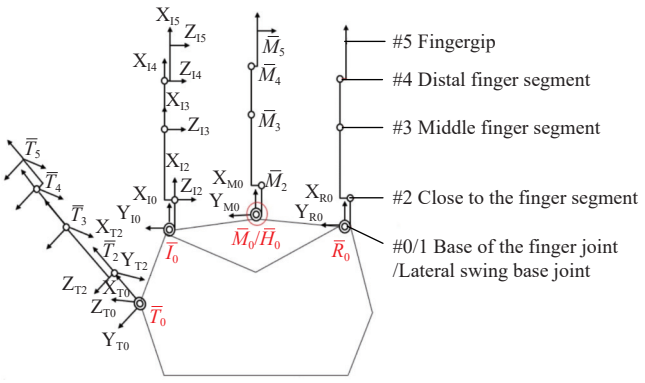

Figure 6 Kinematic model of orchard dexterous hand

Since the dexterous hand adopts a modular design and the joint structure of each finger is similar, only the index finger is analyzed kinematically. The D-H method establishes the kinematic equations from the fingertip coordinate system to the reference coordinate system, and the parameters of each linkage of the fingers are listed in Table 1.

Table 1 Index finger D-H parameter

Coordinate No. i	θ_i/rad	d_i/mm	a_{i-1}/mm	α_{i-1}/rad
1	θ_{I1}	0	0	0
2	θ_{I2}	11	4	$\pi/2$
3	θ_{I3}	42	5.5	0
4	θ_{I4}	42	1	0
5	θ_{I5}	30	5.5	0

The chi-square variation matrix between the two neighboring coordinate systems of each finger was calculated from the D-H parameter table as well as the following equation:

$$ {}^{i-1}_{i}\boldsymbol{T} = \begin{bmatrix} c\theta_i & -s\theta_i & 0 & a_{i-1} \\ s\theta_i c\alpha_{i-1} & c\theta_i c\alpha_{i-1} & -s\alpha_{i-1} & -d_i s\alpha_{i-1} \\ s\theta_i s\alpha_{i-1} & c\theta_i s\alpha_{i-1} & c\alpha_{i-1} & d_i c\alpha_{i-1} \\ 0 & 0 & 0 & 1 \end{bmatrix} \tag{1} $$

According to the right-multiplication rule, the order of the chi-square transformation matrices between the joints represented is multiplied together:

$$ {}^{0}_{5}\boldsymbol{T} = {}^{0}_{1}\boldsymbol{T}^{1}_{2}\boldsymbol{T}^{2}_{3}\boldsymbol{T}^{3}_{4}\boldsymbol{T}^{4}_{5}\boldsymbol{T} \tag{2} $$

Therefore, the positive kinematic equation of the index fingertip concerning the global coordinate system is:

$$ {}^{H}_{I5}\boldsymbol{T} = {}^{H}_{I}\boldsymbol{T}^{0}_{5}\boldsymbol{T} \tag{3} $$

Similarly, the positive kinematic equations for the other three fingers can be derived, as well as the transformation matrices of the base coordinate system of each finger concerning the global coordinate system.

3.2 Inverse kinematics modeling

Inverse kinematics of the index finger means that the spatial coordinates of the fingertip point located under the reference coordinate system of the index finger are known, and a series of individual joint angles that satisfy the desired requirements are computed, i.e., specific values of θ_1, θ_2, θ_3, and θ_4 are obtained.

$$ {}_5^1\boldsymbol{T} = {}_1^0\boldsymbol{T}^{-1}(\theta_1){}_5^0\boldsymbol{T} = {}_2^1\boldsymbol{T}(\theta_2){}_3^2\boldsymbol{T}(\theta_3){}_4^3\boldsymbol{T}(\theta_4){}_5^4\boldsymbol{T}(\theta_5) \tag{4} $$

The equation ${}_1^0\boldsymbol{T}^{-1}(\theta_1)$ can be obtained by multiplying the coordinate system between the index finger joints. Making the elements at each end of the matrix equation correspondingly equal gives

$$ -s\theta_1 p_x + c\theta_1 p_y = -d_2 - d_3 - d_4 - d_5 \tag{5} $$

Solving the above equation gives

$$ \theta_1 = -\arctan\left(\pm\frac{\sqrt{p_x^2+p_y^2-(d_2+d_3+d_4+d_5)^2}}{d_2+d_3+d_4+d_5}\right) + \arctan\left(\frac{p_y}{p_x}\right) \tag{6} $$

According to the above method, the same method solves for θ_2, θ_3, and θ_4.

3.3 Fingertip workspace analysis

Based on the dexterous hand multi-finger kinematic equations and the positional relationship of the fingertips concerning the global coordinate system, the spatial positions of the fingertips at each joint angle are analyzed to obtain the workspace described by the set of positional points. Combined with the joint angle range of motion, Matlab software is used to solve and simulate the workspace of the fingertips of each finger of the dexterous hand, and the movement space of the dexterous hand in the orchard is obtained, as shown in Figure 7. The thumb, index, middle, and ring finger position points are shown in blue, red, green, and yellow, respectively. As can be seen, there is an extensive range of movement of the fingertips of each finger, the blue dots overlap with all other colors, and the tips of the thumbs are in contact with the tips of the other fingers. The index finger is coupled to the ring finger with the same lateral swing angle, which shows the same workspace in the plane, while the lateral swing of the fingers forms the fingertip spatial position overlap point. The middle finger has no lateral swing angle, and the fingertip point workspace in the plane shows a planar shape in the plane and a straight line in the plane.

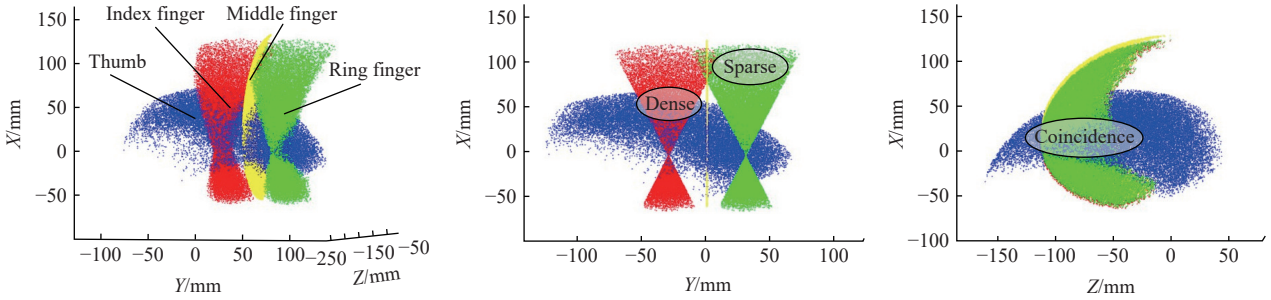

a. Orchard dexterous fingertip movement space

b. Hand XOY workspace

c. Hand XOZ workspace

Figure 7 Orchard dexterous hand movement space

4 Orchard dexterous hand grip model analysis

In order to achieve force-closure grasping with dexterous hands, the problem of finger-object contact needs to be modeled. A friction surface contact model is used, and appropriate mathematical tools describe the relationship between the finger and the grasped object in the configuration during grasping.

Combining the Kapandji test[32] with the resulting workspace allows for visualizing the gesture formation ability of orchard dexterity and assessing the dexterity manipulation ability of dexterous hands. The fit of each finger can be derived from the dexterity fingertip workspace calculated in the previous section. From the overlap of the fingertip space of each finger in Figure 8c, it can be seen that the workspace of the thumb intersects with the workspaces of the index, middle, and ring fingers, which indicates that the thumb fingertip and the other fingertips can contact each other. This also indicates that it has obtained a class rating of level 5 in the Kapandji test, and that it can perform the grasping gestures in the table of classification of the commonly used gestures in the orchard under this rating. Moreover, in Figure 8c, the spatial point of the thumb tip is in contact with the proximal phalangeal joint of the ring finger. A grade rating of 9 can be obtained in the Kapandji test, which indicates that the thumb has excellent mobility and that the orchard dexterous hand has a high degree of dexterity, can form many manipulative gestures, and has a good working ability. The results show that the designed orchard dexterous hand has similar dexterity to a human hand, and the end can reach all points of the designed workspace to meet the gripping requirements for different types of fruits and specialized tools.

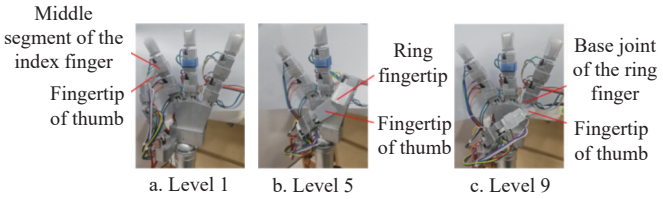

a. Level 1 b. Level 5 c. Level 9

Figure 8 Orchard dexterous hand Kapandji test

4.1 Force-closure determination

In the process of grasping objects with dexterous hands, force-closure is the process of driving reasonable joint torques with dexterous hands to exert certain contact forces, so that a force balance state is formed between the dexterous hands and fruits and vegetables. This ensures that in the process of grasping and picking fruits and vegetables, the objects can be stably grasped in the dexterous hands without slipping, shaking, or damage due to uneven force. It is generally believed that force-closure must meet two conditions. The first is stability. The force of each finger should satisfy the contact model constraints to ensure that the contact position between the finger and the object does not slide relative to each other. The second is anti-interference. The combined force of the dexterous hand on the object can balance any external force interference on the object. The judgment of grasping in this paper is all satisfied with force-closure. The necessary and sufficient conditions for force-closure are:

1) Grasping matrix $\boldsymbol{G}$ has full row rank;

2) Contact force satisfies the contact model constraints.

4.2 Simplification and modeling of the problem

The contact surface between the citrus peel and the finger has unique geometrical and material properties, and the contact area varies with the course of the contact force and is a region of variable shape and size. Therefore, the citrus peel cannot be considered as a rigid object to constrain, and the contact region cannot be reduced to a single contact point.

The dexterous hand takes an envelope grasp to constrain the object, and there are a total of N contact regions between the dexterous hand and the citrus. These contact areas can transmit three forces: the normal pressure P_Z, the frictional forces Q_X and Q_Y in both directions, and the rotational moments M_X, M_Y, and M_Z around the X, Y, and Z axes, as shown in Figure 9.

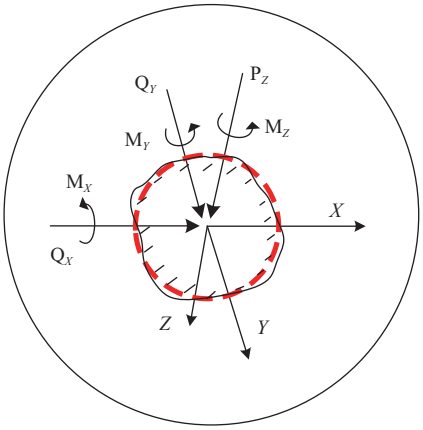

Figure 9 Schematic representation of the contact area

When a friction surface contact constraint is between a finger and a mandarin orange, we make the following assumptions in order to make the analytical problem relatively simple, ignoring some of the uncertainties:

Assumption 1: The contact region can be approximately equated to a circle;

Assumption 2: The contact region changes during the wide range of changes in the external load and is constant during the small perturbation of the external load.

The kinematic and mechanical constraints are investigated regarding the kinematic constraints and force relationships between the dexterous hand and the citrus peel surface contact, respectively. The corresponding coordinate schematic is established as shown in Figure 10, where $\boldsymbol{U}$ is the global coordinate system; $\boldsymbol{W}$ is the citrus coordinate system, located at the center of gravity of the citrus; $\boldsymbol{F}_i$ is the dexterous hand finger coordinate system; and $\boldsymbol{C}_{Wi}$ and $\boldsymbol{C}_{Fi}$ are contact coordinate systems, respectively located at the centers of the contact areas of the citrus and the dexterous hand.

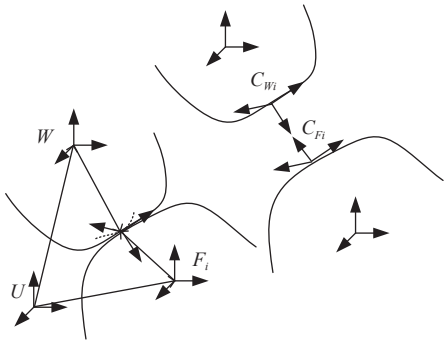

Figure 10 Schematic of coordinates between contacting objects

Suppose $\dot{\boldsymbol{X}}_{\boldsymbol{W}} = [\boldsymbol{v}_w \ \ \boldsymbol{\omega}_w]^{\mathrm{T}}$ and $\dot{\boldsymbol{X}}_{Fi} = [\boldsymbol{v}_{Fi} \ \ \boldsymbol{\omega}_{Fi}]^{\mathrm{T}}$ are the motion spirals of the origin in the global coordinate system in the citadel coordinate system and the dexterity coordinate system, respectively, where $\boldsymbol{v}_w$ and $\boldsymbol{\omega}_w$ are the velocities and angular velocities of the origin in the citadel coordinate system in the global coordinate system, and $\boldsymbol{v}_{Fi}$ and $\boldsymbol{\omega}_{Fi}$ are the velocities and angular velocities of the origin in the dexterity coordinate system in the global coordinate system. Then the velocity and angular velocity of the origin in the contact coordinate system with respect to the global coordinate system can be expressed as:

$$^{C_{Wi}}\dot{\boldsymbol{X}}_{\boldsymbol{C}_{Wi}} = \boldsymbol{A}\left(\boldsymbol{T}_{\boldsymbol{WC}_{Wi}}\right)\boldsymbol{A}\left(\boldsymbol{T}_{\boldsymbol{UW}}^{-1}\right)\dot{\boldsymbol{X}}_{\boldsymbol{W}} \tag{7}$$

$$^{C_{Fi}}\dot{\boldsymbol{X}}_{\boldsymbol{C}_{Fi}} = \boldsymbol{A}\left(\boldsymbol{T}_{\boldsymbol{F}_i\boldsymbol{C}_{Fi}}\right)\boldsymbol{A}\left(\boldsymbol{T}_{\boldsymbol{UF}i}^{-1}\right)\dot{\boldsymbol{X}}_{Fi} \tag{8}$$

Keeping the contact coordinate system on the dexterous hand and the contact coordinate system on the citrus coincident at the time of contact, the velocity constraint can be expressed as:

$$\boldsymbol{H}\left(^{C_{Wi}}\dot{\boldsymbol{X}}_{\boldsymbol{C}_{Wi}} - ^{C_{Fi}}\dot{\boldsymbol{X}}_{\boldsymbol{C}_{Fi}}\right) \geq 0 \tag{9}$$

where, $\boldsymbol{H} = [0 \ \ 0 \ \ 1 \ \ 0 \ \ 0 \ \ 0]$.

Assuming that a coordinate system is established at any point of contact in the contact area, the position vector is $\boldsymbol{p}$, the coordinate system attitude and the contact area center coordinate system are identical, and the velocity at any point of the contact area can be expressed as:

$$\dot{\boldsymbol{x}}_{pw} = \boldsymbol{H}_p^{\mathrm{T}} \cdot ^{C_{Wi}}\dot{\boldsymbol{X}}_{\boldsymbol{C}_{Wi}} \tag{10}$$

$$\dot{\boldsymbol{x}}_{pF} = \boldsymbol{H}_p^{\mathrm{T}} \cdot ^{C_{Fi}}\dot{\boldsymbol{X}}_{\boldsymbol{C}_{Fi}} \tag{11}$$

where, $\boldsymbol{H}_p^{\mathrm{T}} = [\boldsymbol{I} \ \ \hat{\boldsymbol{p}}]^{\mathrm{T}}$.

4.3 Rational equivalence of distributed contact forces

Assuming that the contact is in the elastic deformation stage, the pressure distribution in the contact region is parabolic in shape, the horizontal distance of $\boldsymbol{p}$ from the force $\boldsymbol{F}$ at any point in the contact region is r, the curvature of the dexterous hand in the contact surface is $\frac{1}{R_1}$, the curvature of the citrus peel is $\frac{1}{R_2}$, the depth of indentation is d, and the radius of the contact is a, which will be equated to the contact of a sphere with a flat surface, which has the curvature of the sphere:

$$\frac{1}{R} = \frac{1}{R_1} + \frac{1}{R_2} \tag{12}$$

The contact region force $\boldsymbol{F}$ is related to the plunging depth d as:

$$\boldsymbol{F} = \frac{4}{3}E^* R^{1/2} d^{3/2} \tag{13}$$

where, $\frac{1}{E^*} = \frac{1-v_1^2}{E_1} + \frac{1-v_2^2}{E_2}$, E_1, and E_2 are the modulus of elasticity of the dexterous hand and citrus epidermis, respectively, and v_1 and v_2 are the Poisson's ratios of the dexterous hand and citrus epidermis. Take $E_1 = 1404.70$ MPa, $E_2 = 9.84$ MPa, $v_1 = 0.30$, $v_2 = 0.47$.

The contact radius a is:

$$a = \sqrt{Rd} \tag{14}$$

Then the positive pressure at r is:

$$\boldsymbol{F}_{pr} = \frac{1}{\pi} \cdot \left(\frac{6FE^{*2}}{R^2}\right)^{1/3} \left(1 - \frac{r^2}{Rd}\right)^{1/2} \tag{15}$$

4.4 Obtain the equilibrium equation

The mass of the mandarin is m, and due to the deformation of the mandarin and the dexterous hand, the dexterous hand and the

mandarin are constrained by 13 face contacts. Assuming that the equivalent contact points are $\boldsymbol{C}_i$ (where i = 1, 2, …, 13), $\boldsymbol{U}$ is the inertial coordinate system, and coordinate systems $\boldsymbol{B}$ and $\boldsymbol{F}_j$, $j=1,2$ in citrus and dexterous hands, respectively. The citrus contact coordinate system $\boldsymbol{C}_{Bi}$ is defined at the contact point $\boldsymbol{C}_i$; n_i is the inner normal vector direction at the contact point; $t_i, \boldsymbol{\tau}_i$ is the tangent direction at the contact point $\boldsymbol{C}_i$; and $\boldsymbol{C}_{Fi}$ is the dexterous hand contact coordinate system on the dexterous hand surface, defining z_i as the normal vector direction at the dexterous hand contact point $\boldsymbol{C}_i$, and x_i, y_i as the tangent direction at the contact point $\boldsymbol{C}_i$.

The spin of the contact force on the citrus at the contact point $\boldsymbol{C}_i$ is defined as:

$$\boldsymbol{F}_{C_i}^{C_{Bi}} = \begin{bmatrix} \boldsymbol{f}_{C_i}^{C_{Bi}} \\ \boldsymbol{\tau}_{C_i}^{C_{Bi}} \end{bmatrix} = [\boldsymbol{f}_{ti} \quad \boldsymbol{f}_{\tau i} \quad \boldsymbol{f}_{ni} \quad \boldsymbol{\tau}_{ti} \quad \boldsymbol{\tau}_{\tau i} \quad \boldsymbol{\tau}_{ni}]^{\mathrm{T}} \tag{16}$$

Mapping between the contact point coordinate system on the citrus to the global coordinate system:

$${}_{C_{Bi}}^{G}\boldsymbol{T} = {}_{b}^{G}\boldsymbol{T}\,{}_{C_{Bi}}^{B}\boldsymbol{T} = \begin{bmatrix} {}_{C_{Bi}}^{G}\boldsymbol{R} & \boldsymbol{r}_{C_{Bi}}^{G} \\ 0 & 1 \end{bmatrix} \tag{17}$$

Take the adjoint matrix to map the force spins in the local coordinate system to the global coordinate system:

$$\boldsymbol{F}_{C_i}^{U} = \boldsymbol{A}^{\mathrm{T}}\left({}_{C_{Bi}}^{U}\boldsymbol{T}^{-1}\right)\boldsymbol{F}_{C_i}^{C_{Bi}} \tag{18}$$

$$\boldsymbol{A}^{\mathrm{T}}\left({}_{C_{Bi}}^{U}\boldsymbol{T}^{-1}\right) = \begin{bmatrix} {}_{C_{Bi}}^{U}\boldsymbol{R} & 0 \\ \hat{r}_{C_{Bi}C_{Bi}}^{U}\,{}_{C_{Bi}}^{U}\boldsymbol{R} & {}_{C_{Bi}}^{U}\boldsymbol{R} \end{bmatrix} \tag{19}$$

$$\boldsymbol{F}_{C_i}^{U} = \begin{bmatrix} {}_{C_{Bi}}^{U}\boldsymbol{R}\boldsymbol{f}_{C_i}^{C_{Bi}} \\ \hat{r}_{C_{Bi}C_{Bi}}^{U}\,{}_{C_{Bi}}^{U}\boldsymbol{R}\boldsymbol{f}_{C_i}^{C_{Bi}} + {}_{C_{Bi}}^{U}\boldsymbol{R}\boldsymbol{\tau}_{C_i}^{C_{Bi}} \end{bmatrix} \tag{20}$$

The mechanical equilibrium equation for citrus can be listed as:

$$\sum_{i=1}^{13}\boldsymbol{F}_{C_i}^{U} + \boldsymbol{w} = 0 \tag{21}$$

The grasp matrix is derived as:

$$\boldsymbol{G}\boldsymbol{\lambda} + \boldsymbol{w} = 0 \tag{22}$$

where,

$$\boldsymbol{G} = \begin{bmatrix} \boldsymbol{G}_1 & \boldsymbol{G}_2 & \cdots & \boldsymbol{G}_{13} \end{bmatrix},$$

$$\boldsymbol{\lambda} = \begin{bmatrix} \boldsymbol{\lambda}_1^{\mathrm{T}} & \boldsymbol{\lambda}_2^{\mathrm{T}} & \cdots & \boldsymbol{\lambda}_{13}^{\mathrm{T}} \end{bmatrix}^{\mathrm{T}}$$

$$\boldsymbol{G}_i = \begin{bmatrix} \boldsymbol{t}_i & \boldsymbol{\tau}_i & \boldsymbol{n}_i & 0 & 0 & 0 \\ \boldsymbol{r}_i \times \boldsymbol{t}_i & \boldsymbol{r}_i \times \boldsymbol{\tau}_i & \boldsymbol{r}_i \times \boldsymbol{n}_i & \boldsymbol{t}_i & \boldsymbol{\tau}_i & \boldsymbol{n}_i \end{bmatrix}$$

$$\boldsymbol{\lambda}_i = \boldsymbol{F}_{C_i}^{C_{fi}} = \begin{bmatrix} \boldsymbol{f}_{ti} & \boldsymbol{f}_{\tau i} & \boldsymbol{f}_{ni} & \boldsymbol{\tau}_{ti} & \boldsymbol{\tau}_{\tau i} & \boldsymbol{\tau}_{ni} \end{bmatrix}^{\mathrm{T}}$$

4.5 Contact deformation about hand-citrus movement

Assuming that no sliding or rolling occurs at the point of contact between the dexterous hand and the object, it is considered that they are bonded small contact surfaces that can transmit three directional forces and three directional moments and that the dexterous hand and the mandarin orange move relative to each other through the deformation of the point of contact.

The mapping relationship between the two contact coordinates is:

$${}_{C_{Bi}}^{C_{fi}}\boldsymbol{T} = {}_{F_j}^{C_{fi}}\boldsymbol{T}\,{}_{U}^{F_j}\boldsymbol{T}\,{}_{B}^{G}\boldsymbol{T}\,{}_{C_{Bi}}^{B}\boldsymbol{T} \tag{23}$$

In the ideal state where no deformation occurs, the two contact coordinates at the point of contact are coincident with each other:

$${}_{C_{Bi}}^{C_{fi}}\boldsymbol{T} = \boldsymbol{I} \tag{24}$$

After localized deformation of the mandarin in the contact area, the mandarin position and dexterous hand joint angle are adjusted accordingly to keep the contact position unchanged:

$${}_{C_{Bi}}^{C_{fi}}\boldsymbol{T} = {}_{F_i}^{C_{fi}}\boldsymbol{T}\,{}_{U}^{F_i}\boldsymbol{T}\Delta_{U}^{F_i}\boldsymbol{T}\,{}_{B}^{G}\boldsymbol{T}\Delta_{B}^{G}\boldsymbol{T}\,{}_{C_{Bi}}^{B}\boldsymbol{T}\Delta_{C_{Bi}}^{B}\boldsymbol{T} = \boldsymbol{I} \tag{25}$$

Gives a first-order approximation there:

$$\Delta_{U}^{F_i}\boldsymbol{T} + \Delta_{B}^{U}\boldsymbol{T} + \Delta_{C_{Bi}}^{B}\boldsymbol{T} = 0 \tag{26}$$

Change in attitude of citrus contact coordinate system due to contact deformation:

$$\Delta\boldsymbol{X}_{ci}^{C_{Bi}} = [\Delta\boldsymbol{x}_{ci} \quad \Delta\boldsymbol{y}_{ci} \quad \Delta\boldsymbol{z}_{ci} \quad \Delta\boldsymbol{\theta}_{xci} \quad \Delta\boldsymbol{\theta}_{yci} \quad \Delta\boldsymbol{\theta}_{zci}]^{\mathrm{T}} \tag{27}$$

The differential motion of the contact coordinate system maps to the global coordinate system there:

$$\Delta\boldsymbol{X}_{ci}^{G} = \boldsymbol{A}(\boldsymbol{T})\Delta\boldsymbol{X}_{ci}^{C_{Bi}} = \begin{bmatrix} \boldsymbol{R} & \hat{\boldsymbol{r}}\boldsymbol{R} \\ 0 & \boldsymbol{R} \end{bmatrix}\Delta\boldsymbol{X}_{ci}^{C_{Bi}} \tag{28}$$

The citrus gesture produces small changes assuming that:

$$\Delta\boldsymbol{X}_{w}^{B} = [\Delta\boldsymbol{x}_{w} \quad \Delta\boldsymbol{y}_{w} \quad \Delta\boldsymbol{z}_{w} \quad \Delta\boldsymbol{\theta}_{xw} \quad \Delta\boldsymbol{\theta}_{yw} \quad \Delta\boldsymbol{\theta}_{zw}]^{\mathrm{T}} \tag{29}$$

The change in the contact coordinate system position due to the change in citrus attitude is:

$$\Delta\boldsymbol{X}_{ci}^{CBi} = \boldsymbol{G}_i^{\mathrm{T}}\Delta\boldsymbol{X}_{w}^{B} \tag{30}$$

Dexterous hand joints will produce small movement changes, joint micro-movements for:

$$\Delta\boldsymbol{q} = [\Delta\boldsymbol{q}_1 \quad \Delta\boldsymbol{q}_2 \quad \Delta\boldsymbol{q}_3 \quad \Delta\boldsymbol{q}_4]^{\mathrm{T}} \tag{31}$$

The change in attitude that causes the citrus coordinate system is assumed to be:

$$\Delta\boldsymbol{X}_{Fi} = \left[\Delta\boldsymbol{x}_{Fi} \quad \Delta\boldsymbol{y}_{Fi} \quad \Delta\boldsymbol{z}_{Fi} \quad \Delta\boldsymbol{\theta}_{xFi} \quad \Delta\boldsymbol{\theta}_{yFi} \quad \Delta\boldsymbol{\theta}_{zFi}\right]^{\mathrm{T}} \tag{32}$$

where, $[\Delta\boldsymbol{x}_{Fi} \quad \Delta\boldsymbol{y}_{Fi} \quad \Delta\boldsymbol{z}_{Fi}]^{\mathrm{T}} = \boldsymbol{J}_i\Delta\boldsymbol{q}$, $\Delta\boldsymbol{\theta}_{xFi} = 0, \Delta\boldsymbol{\theta}_{yFi} = 0, \Delta\boldsymbol{\theta}_{zF1} = \Delta\boldsymbol{q}_1 + \Delta\boldsymbol{q}_2$, $\Delta\boldsymbol{\theta}_{zF2} = \Delta\boldsymbol{q}_3 + \Delta\boldsymbol{q}_4$.

The change in attitude from citrus leads to a change in the attitude of the dexterous hand touching the coordinate system as:

$$\Delta\boldsymbol{X}_{Fci} = \boldsymbol{L}_i^{\mathrm{T}}\Delta\boldsymbol{X}_{Fi} \tag{33}$$

$$\boldsymbol{L}_i = \begin{bmatrix} \boldsymbol{x}_i & \boldsymbol{y}_i & \boldsymbol{z}_i & 0 & 0 & 0 \\ \boldsymbol{r'}_i \times \boldsymbol{x}_i & \boldsymbol{r'}_i \times \boldsymbol{y}_i & \boldsymbol{r'}_i \times \boldsymbol{z}_i & \boldsymbol{x}_i & \boldsymbol{y}_i & \boldsymbol{z}_i \end{bmatrix} \tag{34}$$

To simplify the research problem, it is assumed earlier that there is no sliding or contact disengagement problem at the contact, and the two contact coordinate systems are always consistent:

$$\Delta\boldsymbol{X}_{Bci}^{G} + \Delta\boldsymbol{X}'_{Bci} = \Delta\boldsymbol{X}_{Fci} \tag{35}$$

Therefore, the deformation generated at the contact position is:

$$\Delta\boldsymbol{X}_{Bci}^{G} = \Delta\boldsymbol{X}_{Fci} - \Delta\boldsymbol{X}'_{Bci} \tag{36}$$

$$\Delta\boldsymbol{X}_{ci}^{C_{Bi}} = \boldsymbol{A}^{-1}\left({}_{C_{fi}}^{G}\boldsymbol{T}\right)\left(\boldsymbol{G}_i^{\mathrm{T}}\Delta\boldsymbol{X}_{w} - \boldsymbol{L}_i^{\mathrm{T}}\Delta\boldsymbol{X}_{Fi}\right) \tag{37}$$

5 Prototype experiment

The orchard dexterous hand prototype is shown in Figure 11, and the main body is 3D printed from SZUV-W8001P photosensitive resin.

The orchard dexterous hand experimental platform is shown in Figure 12, mounted on the end of a four-degree-of-freedom robotic arm. The control system of the orchard dexterous hand is shown in Figure 13; a feed-forward-based PID control system controls the orchard dexterous hand. Firstly, the control program is written in

the upper computer with Arduino software, and then it is downloaded to the lower computer, running the real-time system for execution through the CAN interface. The RDC501 rotary position sensor acquires finger joint signals and inputs them to the upper computer, which gets the deviation angle, transmits the data, and controls the N20-1218 DC geared motor to rotate to the desired angle through the L9110S four-channel motor driver board to complete the control system of the orchard dexterous hand.

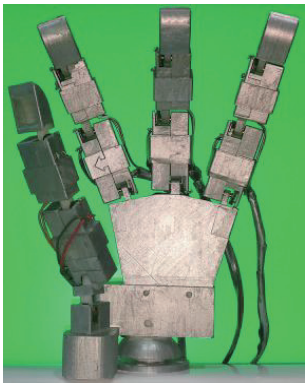

Figure 11 Orchard dexterous hand prototype

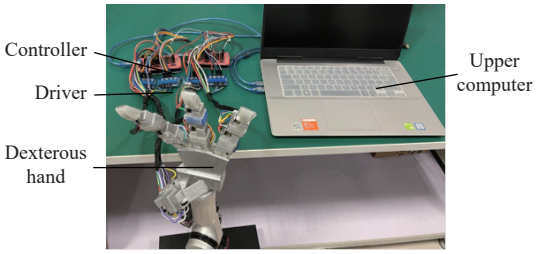

Figure 12 Orchard dexterous hand experiment platform

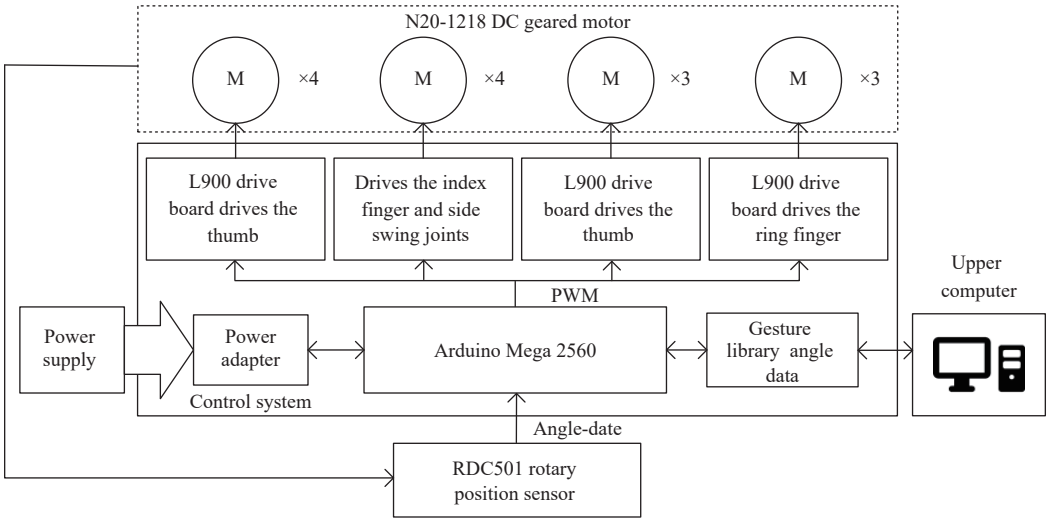

Figure 13 Orchard dexterous hand control system

5.1 Orchard gesture formation and grasping experiments

In order to verify the dexterous hand's ability to form all the gestures in the classification table of common gestures in the orchard and realize the stable grasping of typical fruits and tools, the orchard gesture formation and grasping experiments were conducted. Stable grasping ability is defined as the dexterous hand maintains contact with the target object without slipping in the contact area in the orchard operation scenario. Stable grasping ability is evaluated by two quantitative indices: static stability is the grasping ability of the dexterous hand to maintain the target object without slipping in the stationary state, and dynamic stability is the grasping ability of the dexterous hand to resist external perturbations and maintain the target object. The test methods and judgment bases of the two quantitative indices are as follows:

1) Static stability: The magnitude of the motor current of each joint of the dexterous hand is obtained in real time within one minute after grasping. When there exists a joint motor current exceeding $\left|\mathrm{I}\pm 0.2\mathrm{I}\right|$, it is judged to be slippage and does not satisfy static stability, where I is the initial moment current.

2) Dynamic stability: The robotic arm in the horizontal, longitudinal, and vertical directions, respectively, should maintain 1.8 m/s^2 acceleration throughout a movement of 0.3 m. If the target object does not slip or slip down, it is considered to meet dynamic stability.

The specific parameters of the target objects are listed in Table 2, including different sizes of fruits and tools commonly found in orchards.

Table 2 Object parameters

Grasping gesture	Target object	Size/mm	Mass/g
Two fingers pinch	cherry tomato	*D*:26	11
Three fingers pinch	Small citrus	*D*:38	40
Four fingers pinch	Large citrus	*D*:61	138
Three finger grasp	Large citrus	*D*:61	138
Four finger grasp	ugly orange	*D*:90	283
Palm grasp	Small citrus	*D*:58	132
Four finger grasp	dendrite	*D*:8	150
Three finger grasping tool	scissor	*L*:170, *W*:12, *H*:100	69
Four finger grasping tool	pruning shears	*L*:200, *W*:19, *H*:110	159

In Table 2, *D* is the diameter of the target, *L* is the length of the target, *W* is the width of the target, and *H* is the height of the target.

As shown in Figure 14, the corresponding gesture library information is formed corresponding to the nine groups of grasping gestures. Each group of gestures goes through three repetitions of the test. Each test contains a static and dynamic stability test. N is the number of tests, and N_s is the number of grasping successes. The grasping success rate reflects the ability of the dexterous hand under different gestures to stabilize the grasping. The grasping success rate can be expressed as:

$$S = \frac{N_s}{N} \times 100\% \tag{38}$$

Table 3 Knuckle contact force under different grasping gestures

Finger	Finger segment	Serial number	Pinch with three fingers/ N	Pinch with four fingers/ N	Three-finger enveloping grasp/ N	Four-finger enveloping grasp/ N
Thumb	Fingertip	1	1.92	2.13	0.73	0.89
	Distal digital segment	2			0.72	0.56
	Proximal digital segment	3			1.71	3.64
Index finger	Fingertip	4	0.37	0.35	0.53	0.94
	Distal digital segment	5			0.34	0.63
	Proximal digital segment	6			0.54	0.87
Middle finger	Fingertip	7	0.76	0.64	1.61	0.91
	Distal digital segment	8			0.62	0.47
	Proximal digital segment	9			0.47	0.43
Ring finger	Fingertip	10		0.43		0.56
	Distal digital segment	11				1.92
	Proximal digital segment	12				0.25
Palm	Palm	13			1.21	2.20

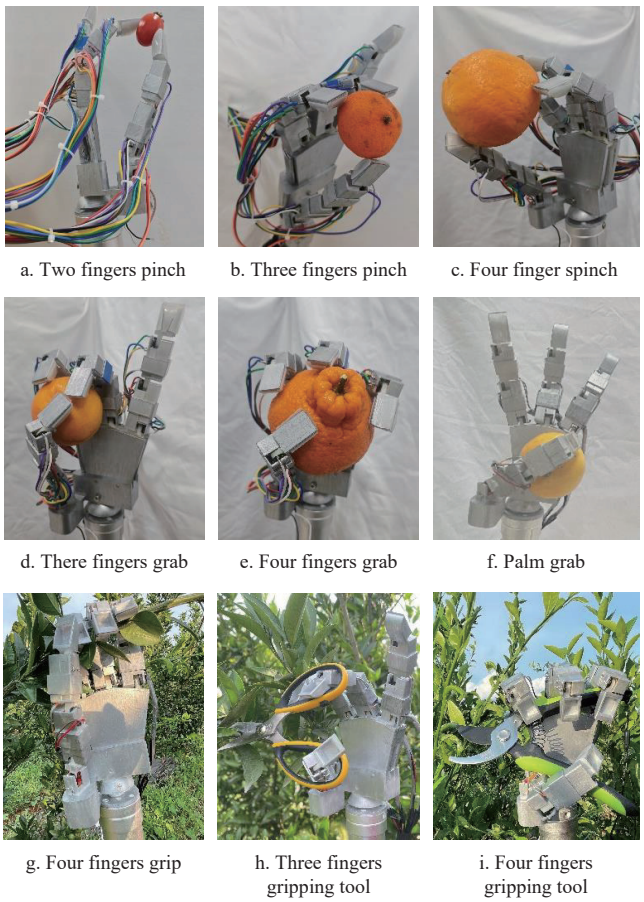

a. Two fingers pinch b. Three fingers pinch c. Four finger spinch

d. There fingers grab e. Four fingers grab f. Palm grab

g. Four fingers grip h. Three fingers gripping tool i. Four fingers gripping tool

Figure 14 Experiment on gesture formation of dexterous hand

The experimental results show that only group g had a 0% success rate in gesture branch grasping, while the rest of the groups had a 100% success rate in branch grasping. The reason for the failure of group g is that the diameter of the branch is only 8 mm, and due to the limitation of the angle range of some finger joints, the fingers could not effectively contact the main body of the branch, but only touched the leaves on the branch, which formed a potentially unstable grasping state. The unstable gripping state is easily broken by wind interference and machine movement in unstructured agricultural environments, which ultimately leads to gripping failure. The dexterous hand can grasp a diameter of 26-90 mm, a mass of 11-238 g spherical fruit, and all kinds of special orchard work tools. The orchard dexterous hand can grasp different types of objects with gestures similar to those of a human hand, and the design of independent actuation of each joint enables the orchard dexterous hand to present a wider variety of grasping postures. At the same time, fingers not involved in gesture formation can be positionally controlled as needed, allowing the orchard dexterous hand to grasp in a more appropriate spatial stance, reducing interference in gesture formation. By grasping objects of different shapes and different grasping requirements in the orchard, it can be seen that the dexterous hand has stable grasping ability and high flexibility, reflecting good versatility and adaptability.

5.2 Contact force test experiment

In the process of fruit picking, the dexterous hand first grasps and fixes the fruit to provide sufficient friction for the separation of fruit stalks and, at the same time, to avoid fruit damage, so the normal pressure of the dexterous hand on the fruit needs to satisfy certain conditions. Different regular forces are generated for grasping gestures, and separate measurements of the normal forces allow for finger contact force analysis.

The FSR402 resistive thin-film pressure sensor measures the amount of contact force by placing it against the knuckle. The experimental grasping target is a navel orange from the citrus base of Huazhong Agricultural University. The shape is nearly oval, the mass is 234 g, the long diameter is 79 mm, the short diameter is 71 mm, the grasping position is the navel orange long diameter axis pointing to the palm of the dexterous hand, the grasping point is distributed in the maximum cross-section perpendicular to the long axis when pinching accurately, and the thumb and the middle finger are in the opposite to top pinching posture when enveloping grasping. The orchard dexterous hand contact force test experiment is shown in Figure 15.

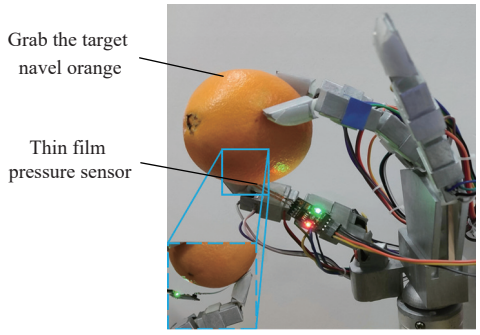

Figure 15 Orchard dexterous hand experiment platform

Designed to grasp the same navel orange under four different gestures, the data from the knuckle pressure sensors were collected three times and averaged. The magnitude of the contact force of each knuckle under different grasping gestures of the dexterous hand is listed in Table 3, while Figure 16 shows the comparison of contact forces.

The contact force of the thumb tip was the largest under the pinching gesture, followed by the middle finger. The rest of the knuckles played an auxiliary role because the thumb and the index finger formed an opposable grip. The maximum knuckle contact force under the envelope grasping gesture was more significant than that under the pinching gesture because the contact force of each knuckle was mainly used to overcome the gravity of the navel orange during pinching. In contrast, the number of contacting knuckles increased in envelope grasping, which resulted in a greater

contact force and a more stable grasp. However, the location of contact points under envelope grasping is not easy to determine, and it is challenging to realize precise grasping, while pinch gesture is suitable for precise pinching due to fewer contact points and a simple mechanical model.

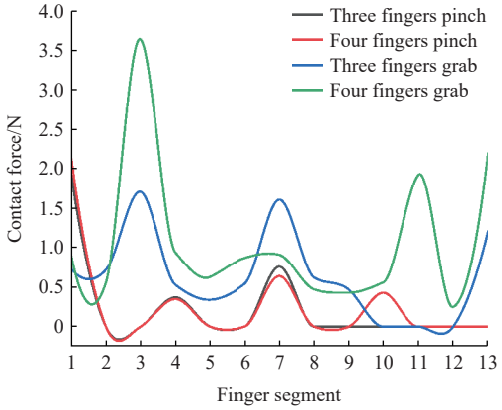

Figure 16 Comparison of contact forces

6 Conclusions

In order to improve the versatility and dexterity of the orchard end actuator, the common gestures in orchard were summarized, and a classification table of orchard grasping gestures was formed. A 14-DOF orchard dexterous hand modeled after the human hand was designed. The dexterous hand has a reasonable structure design, high flexibility, and strong reliability. The forward and inverse kinematics of the finger and the multi-finger kinematics equation were solved, and the fingertip motion space was further calculated, which verified the flexibility of the dexterous hand. Based on the Hertz elastic theory, the equivalent distribution model of the contact force is solved, the gripping matrix is established based on the contact model of the friction surface, and the relationship between the finger and the grasped object is described. The experimental platform of orchard dexterous hand was established, and gesture formation experiment, gripping experiment, and contact force test were carried out. The results showed that the dexterous hand could form various gestures commonly used in orchards, grasp spherical fruits with a diameter of 26-90 mm and a mass of 11-238 g, as well as various special orchard working tools. For a navel orange with a mass of 234 g, the dexterous hand can achieve a stable grasp with different gestures. This provides a theoretical basis and technical support for the realization of orchard compound agronomy.

Acknowledgements

This work was funded by the Hubei Province Technological Innovation Program Project, China (Grant No. 2024BBB060); the 2024 Huazhong Agricultural University Independent Science and Technology Innovation Fund Project, China (Grant No. 2662024GXPY006); and the National Key Research and Development Program, China (Grant No. 2024YFD2300800).

[References]

[1] Zheng Y J, Jiang S J, Chen B T, Lu H T, Wang C, Kang F, et al. Review on technology and equipment of mechanization in hilly orchard. Transactions of the CSAM, 2020; 51(11): 1–20.

[2] Zhao C J. Current situations and prospects of smart agriculture. Journal of South China Agricultural University, 2021; 42(6): 1–7.

[3] Liu C L, Gong L, Yuan J, Li Y M. Current Status and Development Trends of Agricultural Robots. Transactions of the CSAM, 2022; 53(7): 1–22,55.

[4] Zhou J G, Wang Y K, Chen J, Luo T Y, Hu G R, Jia J L, et al. Research hotspots and development trends of harvesting robots based on bibliometric analysis and knowledge graphs. Int J Agric & Biol Eng, 2024; 17(6): 1–10.

[5] Yuan Y W, Bai S H, Niu K, Zhou L M, Zhao B, Wei L G, et al. Research progress on mechanized harvesting technology and equipment for forest fruit. Transactions of the CSAE, 2022; 38(9): 53–63. DOI: 10.11975/j.issn.1002-6819.2022.09. 006.

[6] Jia J M, Ye Y Z, Cheng P L, Zhu Y P, Fu X P, Chen J N. Design and Experimental Optimization of Hand-held Manipulator for Picking Famous Tea Shoot. Transactions of the CSAM, 2022; 53(5): 86–92. DOI: 10.6041/j.issn.1000-1298. 2022.05.009.

[7] Ji J T, Du S C, Li M S, Zhu X F, Zhao K X, Zhang S H, et al. Design and experiment of a picking robot for Agaricus bisporus based on machine vision. Int J Agric & Biol Eng, 2024; 17(4): 67–76.

[8] Wang Z, Wang Q Y, Lou M Z, Wu F, Zhu Y N, Hu D, et al. Geometric based apple suction strategy for robotic packaging. Int J Agric & Biol Eng, 2024; 17(3): 12–20.

[9] Tinoco V, Silva M F, Santos F N, Rocha L F, Magalhaes S, Santos L. A review of pruning and harvesting manipulators. IEEE International Conference on Autonomous Robot Systems and Competitions (ICARSC). IEEE, 2021: pp.155–160.

[10] Pan Y F, Zhou Y, He L, Song L, Song L, Song Z S, Zhu H. Research progress of orchard pruning machine. Journal of Agricultural Mechanization Research, 2023; 45(7): 261–268.

[11] Zahid A, Mahmud M S, Long H, Heinemann P, Choi D, Schupp J. Technological advancements towards developing a robotic pruner for apple trees: A review. Computers and Electronics in Agriculture, 2021; 189: 106383.

[12] Zhou K H, Xia L R, Liu J, Qian M Y, Pi J. Design of a flexible end-effector based on characteristics of tomatoes. Int J Agric & Biol Eng, 2022; 15(2): 13–24.

[13] Lin Y F, Liang H, Tong J H, Shen H Y, Fu X P, Wu C Y. Design and feasibility analysis of a graded harvesting end-effector with the function of soluble solid content estimation. Int J Agric & Biol Eng, 2024; 17(5): 239–246.

[14] Gao J, Zhang F, Zhang J, Yuan T, Yin J, Guo H, et al. Development and evaluation of a pneumatic finger-like end-effector for cherry tomato harvesting robot in greenhouse. Computers and Electronics in Agriculture, 2022; 197: 106879.

[15] Wei B, He J Y, Shi Y, Jiang G L, Zhang X Y, Ma Y. Design and experiment of underactuated end-effector for citrus picking. Transactions of the CSAM, 2021; 52(10): 120–128.

[16] Zahid A, Mahmud M S, He L, Choi D, Heinemann P, Schupp J. Development of an integrated 3R end-effector with a cartesian manipulator for pruning apple trees. Computers and Electronics in Agriculture, 2020; 179: 105837.

[17] Jongpyo J, Jeongin K, Jaehwi S, Jeongeun K, Hyoung S I. Towards an efficient tomato harvesting robot: 3D perception, manipulation, and end-effector. IEEE Access, 2021; 9: 17631–17640.

[18] Zhao Y X, Wan X F, Duo H X. Review of rigid fruit and vegetable picking robots. Int J Agric & Biol Eng, 2023; 16(5): 1–11.

[19] Cai S B, Tao Z C, Wan W W, Yu H Y, Bao G J. Multi-fingered Dexterous Hands: From Simplicity to Complexity and Simplifying Complex Applications. Journal of Mechanical Engineering, 2021; 57(15): 1–14.

[20] Xu Y L, Xu S X, Xu X, Zhao C L, Yang A L. Kinematics and grasping analysis of SHU-II five-finger dexterous hand. Chinese Journal of Scientific Instrument, 2018; 39(9): 30–39.

[21] Deepak R B, Pramod K P, Alok R B. Enhancing dexterous grasping and manipulation through linkage-driven under actuated five-fingered robotic hand: A Computational Approach. International Journal of Mechanical Engineering and Robotics Research, 2024; 13(5): 548–557.

[22] Cao S K, Bao G J, Pan L F, Yang B C, Zhou X Y. Structural and experimental study of a multi-finger synergistic adaptive humanoid dexterous hand. Biomimetics, 2025; 10(3): 155–175.

[23] Melchiorri C, Palli G, Berselli G, Vassura G. Development of the UB hand IV: Overview of design solutions and enabling technologies. IEEE Robotics & Automation Magazine, 2013; 20(3): 72–81.

[24] Tao Z, Sheng S, Chen Z, Bao G. Novel design method for multi-configuration dexterous hand based on a gesture primitives analysis. Industrial Robot: the International Journal of Robotics Research and Application, 2021; 48(3): 463–472.

[25] Kim U, Jung D, Jeong H, Park J, Jung H M, Cheong J, et al. Integrated linkage-driven dexterous anthropomorphic robotic hand. Nature Communications, 2021; 12(1): 7177.8.

[26] Li S, Ma X, Liang H, Görner M, Ruppel P, Fang B, et al. Vision-based teleoperation of shadow dexterous hand using end-to-end deep neural network. International Conference on Robotics and Automation (ICRA). IEEE, 2019; pp.416–422.

[27] Cerulo I, Ficuciello F, LippielloV, Siciliano B. Teleoperation of the SCHUNK S5FH under-actuated anthropomorphic hand using human hand motion tracking. Robotics and Autonomous Systems, 2017; 89: 75–84.

[28] Capsi-Morales P, Barsakcioglu D Y, Catalano M G, Grioli G, Bicchi A, Farina D. Merging motoneuron and postural synergies in prosthetic hand design for natural bionic interfacing. Science Robotics, 2025; 10(98): eado9509.

[29] Piazza C, Grioli G, Catalano M G, Bicchi A. A century of robotic hands. Annual Review of Control Robotics and Autonomous Systems, 2019; 2: 1–32.

[30] Feix T, Bullock I M, Dollar A M. Analysis of human grasping behavior: Correlating tasks, objects and grasps. IEEE Transactions on Haptics, 2014; 7(4): 430–441.

[31] Feix T, Romere J, Schmiedmayer H B, Dollar A M, Kragic D. The grasp taxonomy of human grasp types. IEEE Transactions on Human-Machine Systems, 2015; 46(1): 66–77.

[32] Kapandji A. Clinical test of apposition and counter-apposition of the thumb. Annales de Chirurgie de la Main: Organe Officiel des Societes de Ohirurgie de la Main, 1985; 5(1): 67–73.